Materials Science & Engineering C 113 (2020) 111002

Contents lists available at ScienceDirect

Materials Science & Engineering C

journal homepage: www.elsevier.com/locate/msec

Study of nitrogen implantation in Ti surface using plasma immersion ion implantation & deposition technique as biocompatible substrate for artificial membranes

M. Cisternas[a,b], H. Bhuyan[a,b,*], M.J. Retamal[a,b], N. Casanova-Morales[a,b,f], M. Favre[a,b], U.G. Volkmann[a,b], P. Saikia[a], D.E. Diaz-Droguett[a,b], S. Mändl[c], D. Manova[c], N. Moraga[a,b], A. Chandía-Cristi[d], A. Alvarez[d], F. Guzman[e]

[a] Instituto de Física, Pontificia Universidad Católica de Chile, Av. Vicuña Mackenna 4860, Santiago, Chile
[b] Centro de Investigación en Nanotecnología y Materiales Avanzados (CIEN-UC), Av. Vicuña Mackenna 4860, Santiago, Chile.
[c] Leibniz-Institut of Surface Engineering, Leipzig, Germany
[d] Facultad de Ciencias Biológicas, Pontificia Universidad Católica de Chile, Av. Vicuña Mackenna 4860, Santiago, Chile
[e] Depto. de Física FCFM, Universidad de Chile, Beauchef 850, Santiago, Chile
[f] Present address: Facultad de Artes Liberales, Universidad Adolfo Ibáñez, Santiago, Chile

A B S T R A C T

The present investigation reports the modification of Ti substrates by a plasma technique to enhance their physio-chemical properties as biocompatible substrates for the deposition of artificial membranes. For that purpose, nitrogen ions are implanted into Ti substrate using the plasma immersion ion implantation & deposition (PIII &D) technique in a capacitively coupled radio frequency plasma. The plasma was characterized using optical emission spectroscopy, together with radio frequency compensated Langmuir probe, while the ion current towards the substrate was measured during the implantation process using an opto-electronic device. X-ray photoelectron spectroscopy (XPS) was used for chemical analysis of the surface, confirming the presence of δ-TiN. The penetration depth of the nitrogen ions into the Ti substrate was measured using secondary ions mass spectroscopy (SIMS) while the morphological changes were observed using atomic force microscopy (AFM). A calorimetric assay was used to prove that the TiN samples maintain the biocompatibility of the untreated Ti surface with its native oxide layer. The ion implantation increases the load bearing ability of Ti surface by the formation of α-Ti(N) and δ-TiN phases on the sub-surface of Ti, and maintains the bio compatibility of Ti surface. After the plasma treatment a thin layer of chitosan (CH) was deposited in order to provide a moisturizing matrix for the artificial membrane of 1,2-dipalmitoyl-sn-3- phosphor glycerocholine (DPPC). The CH and subsequently the DPPC were deposited on the plasma deposited TiN substrate by using physical vapor deposition. The formation of artificial membranes was confirmed by AFM, measuring the topography at different temperatures and performing force curves.

1. Introduction

Artificial membranes nowadays gain importance [1–4], because of their model character for the study of the behavior of biological membranes. Biological membranes are composed of phospholipids and proteins that change its behavior due to physical and chemical stimuli. The formation and study of a biocompatible environment, capable to support an artificial membrane without denaturation is an important step for the development of biocompatible biosensors [3,4]. A good candidate to support artificial membranes is titanium (Ti), a biocompatible material widely used in biomedical application [5,6]. To improve the mechanical properties of Ti, while maintaining its biocompatibility benefits for biological systems, one possibility is to provide biocompatible titanium nitride (TiN) coatings [7] on Ti. TiN coating provides both increase roughness and wettability, which is important for surface affinity and cell adherence. Cell attachment, spreading and proliferation are evidently enhanced on TiN coatings [8]. Due to its enhanced mechanical properties, TiN coatings have different application scopes like in joint prostheses, fracture fixation, orthopedic, dentistry, among others [9–11]. Furthermore, TiN based electrodes are promising materials for the fabrication of bendable electronic devices [12] because of its low resistance and high conductivity. Owing to its enhanced mechanical properties, high conductivity and biocompatibility, TiN coating will act as a promising substrate for the development of biosensors, in comparison to pure Ti.

Different plasma based techniques such as inductively coupled plasma assisted physical vapor deposition [13], reactive plasma spraying [14], or direct current magnetron sputtering [15] have been used to produce TiN coatings. In comparison to these techniques, plasma immersion ion implantation & deposition (PIII&D) technique

* Corresponding author at: Instituto de Física, Pontificia Universidad Católica de Chile, Av. Vicuña Mackenna 4860, Santiago, Chile.
E-mail address: hbhuyan@fis.puc.cl (H. Bhuyan).

https://doi.org/10.1016/j.msec.2020.111002
Received 15 May 2018; Received in revised form 10 February 2020; Accepted 20 April 2020
Available online 25 April 2020
0928-4931/

works at low temperature and produces high adhesion strength coatings *via* ion implantation and atomic intermixing [16,17]. It combines excellent bonding strength between the deposited film and substrate with a 3D complex-shape treatment [18].

The aim of the present investigation was to modify a Ti surface to form TiN substrate by PIII&D technique in order to support an artificial membrane of 1,2-dipalmitoyl-sn-3-phosphor glycerocholine (DPPC) on a layer of chitosan. Chitosan (CH) is a linear polysaccharide obtained by the deacetylation of chitin, which can be found in the exoskeleton of insects, shells of crustaceans, fungi and plants, thus being very easy to obtain at low cost. CH has also interesting features, such as biocompatibility [19–21], biodegradability [20,21], non-toxicity [21], and antimicrobial activity [22] among others [23–26]. For these characteristic it has been widely used in many applications, including manufacturing of artificial skin [26], wound healing [27], biosensors [28,29], controlled drug-release [28–30], agriculture [31,32], and water treatment [20]. In the membrane research, CH plays an important role due to its porous nature [33,34] and water insolubility [35,36] that provides the hydration of the artificial membrane [4]. The CH acts as moisturizing matrix for DPPC, which is a widely studied phospholipid [37]. The DPPC has been used like a prototype of biological membranes [38]. The structure and temperature-dependence of the DPPC are well known. The DPPC phases are: crystal phase subgel (L_C), gel phase (L_β), ripple phase (P_β), fluid crystalline (L_α) [1,2] and fluid disordered. Thus, an artificial membrane of DPPC is in a high demand. A biocompatible substrate with high conductivity and load-bearing capacity is a suitable substrate for such a model cell membrane of supported lipid bilayers (SLBs). Therefore, focus has been made to prepare a biocompatible TiN substrate as a platform for the formation of the DPPC membrane. For this nitrogen implantation is done into Ti surface by PIII&D technique in a capacitively coupled radio frequency discharge. This technique usually leads to the formation of two major phases on Ti, the solid solution titanium α-Ti(N) and the cubic δ-TiN phases [39]. These two phases increase the load bearing capacity while maintaining the biocompatibility of Ti surface. The structural and mechanical properties as well as biocompatibility of nitrogen implanted Ti surface have been investigated. Further, the deposition of CH/DPPC on top of nitrogen implanted Ti surface is reported and discussed. It should be mentioned here that to the best of our knowledge, there has been no scientific report on the deposition of CH and subsequently DPPC phospholipid bilayer membrane on TiN substrate by physical vapor deposition (PVD) in combination with a precise thickness control *via* very high resolution ellipsometry.

2. Experimental methods

2.1. Capacitively coupled radio frequency (CCRF) discharge

A CCRF discharge operating at 13.56 MHz is used as a plasma source for the PIII&D technique. An automatic matching network (ENI MWH-5-01) is connected between the RF power supply and the electrodes to deliver maximum power to the plasma. The RF power generator (ENI ACG-6B) can deliver up to 600 W and is equipped for simultaneously monitoring of forward power and reflected power. A schematic diagram of the experimental arrangements for ion implantation and ion current measurement along with the plasma producing system is shown in Fig. 1. An LC circuit is used to protect the RF generator and the matching unit from high voltage pulses. The anode and power electrodes consist of two parallel circular discs separated by 7 cm. The anode, top plate, is 10 cm in diameter and the water-cooled bottom plate, which is powered electrode, is 8 cm in diameter. Bulk plasma is produced and fills the space between the electrodes with the electrodes covered by the plasma sheath regions. Due to the asymmetry of the electrodes, a negative DC potential develops between the bulk plasma and the powered electrode, which is termed as self-bias in a RF plasma. Owing to this self-bias the ion energies near the power electrode reach up to a few hundred eV even without applying additional high voltage pulses.

2.2. Substrate preparation

Titanium substrates, machined from high purity titanium rod purchased from Goodfellow, Cambridge Limited, UK, were polished to a mirror finish with 1 μm diamond paste (using Buehler polisher N°60-1990). The substrates were cleaned in an ultrasonic bath with acetone before being loaded to the CCRF plasma chamber. The average roughness measured with Atomic Force Microscopy (AFM) of the polished Ti substrates is approx. 627 pm. The polished titanium substrates were used for a series of nitrogen PIII&D experiments at fixed 6 kV pulsed voltage (500 Hz and 10 μs pulse width) at a substrate temperature of 550 °C. A movable substrate holder is placed between the two circular shaped discs parallel electrodes of the CCRF plasma chamber, effectively yielding a triode geometry. The sample holder carries an integrated heater and cables for the pulsed voltage supply. To estimate the ion current on the substrate during PIII&D, an opto-electronic insulator system is coupled to the substrate holder. In addition to the traditional substrate cleaning, a pretreatment was done for oxide removal on the substrate surface. For this step pure argon PIII&D was provided at 200 mTorr for 15 min at 50 W RF power with 6 kV pulse voltage and 10 μs pulse width. Subsequently, the pretreated substrate was ion implanted at 50 W RF power using a mixture of nitrogen (80%) and hydrogen (20%) gas at 200 mTorr. The experiments were carried out with different implantation times (1, 2, 3 and 4 h). The substrate temperature was measured by a thermocouple fixed to the substrate surface and is maintained constant at 550 °C during the implantation. The PIII&D process employed for these experiments is different from similar processes reported in the literature as a rather high nitrogen pressure was used, compared to 1–5 mTorr in similar experiments [16,17]. Consequently, a high collision rate with a short mean free path was achieved. When the negative high voltage pulses (with pulse length 10 μs, repetition rate 500 Hz) is switched on, the ions are accelerated across the plasma sheath towards the surface and are implanted.

2.3. Plasma characterization

Optical-emission spectroscopy (OES) was used in order to investigate the ionic, atomic and molecular species present in the plasma during the implantation process. OES was recorded using an Ocean Optics PC2000 300–1000 nm spectrometer. The emission spectral data was collected through a quartz window using a lens system and an optical fiber focusing at the substrate surface. The plasma parameters such as density (n_e), temperature (T_e) and floating potential have been measured using an RF-compensated Langmuir probe. It is connected through a movable feed through and can be positioned along a straight line centred between the two electrodes. The probe tip consists of a tungsten wire of 400 μ*m* diameter and 7 mm length. The compensation of the Langmuir probe is essential in RF discharges. A passive compensation scheme is applied to suppress the RF oscillation of the plasma potential. A parallel resonance circuit blocks the base frequency of 13.56 MHz and all harmonics up to 67.8 MHz. Further compensation is achieved by an external floating electrode, which consists of 20 turns of 0.125 mm diameter tungsten wire around the probe insulator. The floating electrode is connected through a capacitor to a point between the probe tip and the RF compensation circuits.

2.4. Bilayer formation

Low viscosity chitosan (CH) from shrimp shells (de-acetylation degree ≥75%) and DPPC (≥99%) were acquired from Sigma Aldrich (St. Louis, MO and Milwaukee, WI, USA). The CH and the DPPC are evaporated using a Knudsen Cell inside a high vacuum chamber by PVD technique [4]. The CH was evaporated at 0.04 Å/s bottom-up to 75 Å

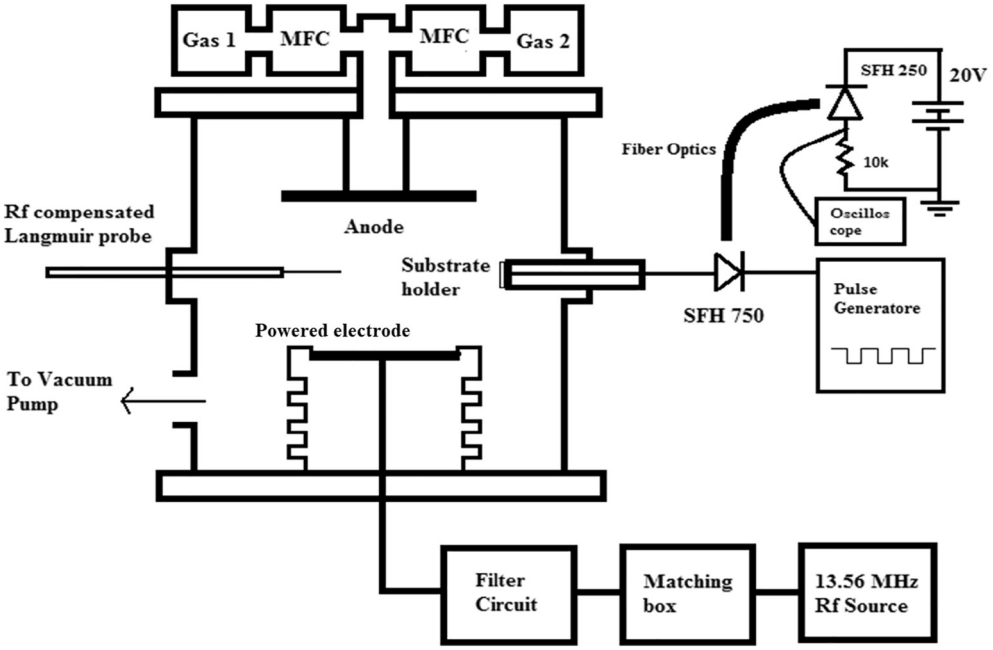

Fig. 1. Schematic diagram of the experimental set-up.

monitored *in situ* with very high resolution ellipsometry (VHRE) over the nitrogen implanted titanium substrate and DPPC was evaporated at 0.08 Å/s bottom up with PVD over the previously evaporated CH.

2.5. Sample characterization

The Ti substrates were investigated before and after the ion implantation process by x-ray photoelectron spectroscopy (XPS), secondary ions mass spectroscopy (SIMS), micro hardness tester and AFM. Chemical analyses were performed by a Physical Electronics model 1257 XPS system using Al Kα emission. Binding energies and oxidation states were obtained from high resolution scans. The binding energy scale was calibrated according to the C 1 s peak (284.8 eV) of spurious carbon at the surface. With SIMS in a time-of-flight setup, it was possible to measure the penetration depth of the nitrogen ions for different implantation times. Ga ions were used for analyzing the pulse with a scan size of 50 × 50 μm^2 at 2 pA. Sputtering was performed with oxygen ions for a crater size of 300 × 300 μm^2 at a current of 800 μA. By measuring the crater depth, the thickness of the nitrided layers was determined by assuming a linear sputter rate with no degradation of the profile edges due to sputter roughening within the crater. The hardness of the Ti surface was measured before and after ion implantation using a Vickers Leco Hardness Testing Machine M-400-H (DIN EN ISO 14577) for loads of 10 to 500 mN. With this technique, it was possible to observe differences in the surface hardness of the samples as a function of implantation time. The morphology of Ti surface before and after the ion implantation process and CH/DPPC depositions were observed using an AFM (NanoWizard 3 BioScience from JPK). AFM force curve measurements on the DPPC membrane were performed using gold covered silicon tips with a curvature radius of 10 nm, resonance frequency of ~300 kHz and force constant of ~50 N/m (PPP-NCHAuD from NanoAndMore).

2.6. Biocompatibility test

Biocompatibility test were performed only for the Ti and nitrogen implanted Ti surfaces, as the CH and the DPPC are already known biocompatible materials. For the biocompatibility test, the cultures of C3H 10T1/2 cells were donated by Enrique Brandan (Pontificia Universidad Católica de Chile, Santiago, Chile). C3H 10 T1/2 cells were maintained in Dulbecco's medium (DMEM) supplemented with 10% fetal bovine serum, 100 IU/ml penicillin, and 100 μg/ml streptomycin. For the cell viability test the embryonic fibroblast cell line C3H 10T1/2 was used. The cells were seeded at 5 × 10^3 cell/100 ml on the Ti and TiN surfaces with DMEM medium supplemented during 24 h, after which the cell viability was measured by 3-(4,5-dimethylthiazol-2-yl)-5-(3-carboxymethoxyphenyl)-2-(4-sulfophenyl)-2H-tetrazolium (MTS) assay [40]. After 2 h of incubation with MTS, a purple color developed within the cells, indicating the cleavage of the tetrazolium salt by mitochondrial reductase in living cells. The purple product (formazan products that are directly soluble in cell culture medium) was measured at 492 nm using an enzyme-linked immunosorbent assay (ELISA) reader (Autobio PHOmo). The percent reduction of MTT was compared to controls cells not exposed to the material, which represented 100% MTT reduction.

3. Results and discussion

3.1. Measurement of discharge parameters

The characterization of the plasma during the implantation process was done using optical emission spectroscopy (OES). This technique allows identifying the ions species and its ionization degrees of the particles that compose the plasma. The plasma is composed principally of atomic and molecular nitrogen in neutral (0) and ionized state (+1). With the optoelectronic device, it was possible to determine roughly the ion flux at the surface for each pulse applied onto the substrate during PIII&D. Due to the expected, low ionization degree (only +1 and no +2 has been observed), it is possible to assume that all current incoming to the substrate from the plasma is due to the singly charged ions. The flux obtained per pulse was approximately 3.8 × 10^{15} cm^{-2} s^{-1}. It is worthwhile to mention that in this current measurement both the dominating secondary electron current and the displacement current are included so the obtained flux is larger than the expected value [16]. At the same time, energetic ions will bombard the surface during the pulse pauses, so that the effective ion flux will be even higher [41].

The bulk plasma density was measured by the RF compensated Langmuir probe. The shift of logarithmic electron current curve of the compensated to the uncompensated probe is found to approximately 3.05 V. This amounts to the oscillation amplitude of plasma potential.

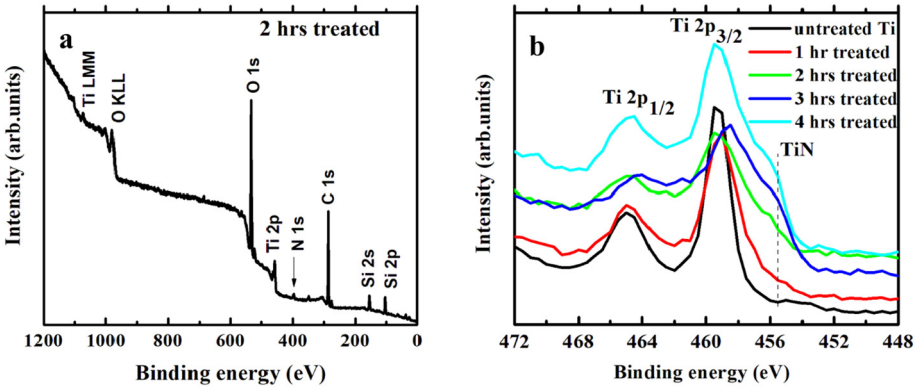

Fig. 2. (a) Representative XPS spectrum of broad energy scan acquired from the 2 h treated sample and (b) XPS spectra corresponding to Ti 2p photoelectron signal for untreated titanium and 1 to 4 h treated sample.

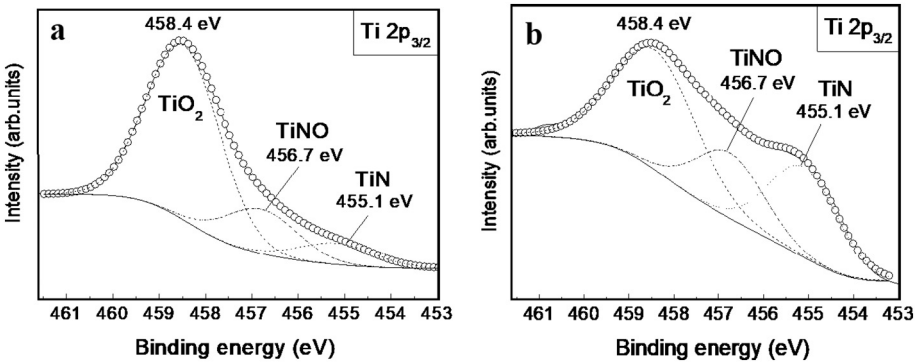

Fig. 3. High-resolution XPS spectra of Ti $2p_{3/2}$ for the sample implanted for (a) 1 h duration and (b) 3 h duration.

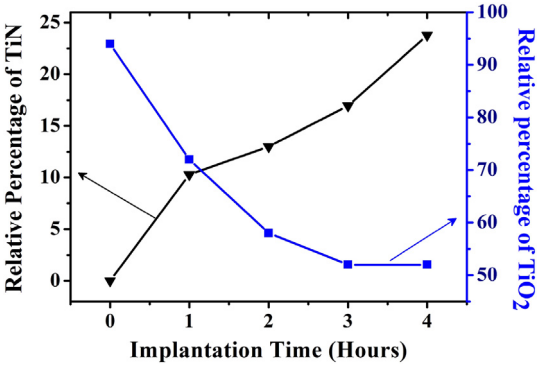

Fig. 4. Relative percentage of TiN and TiO_2 with implantation time, obtained from their corresponding high resolution Ti $2p_{3/2}$ spectra.

Therefore, according to Oksuz et al. [42] the estimation of electron temperature from the inverse slope of the linear part of the logarithmic electron current is valid in our case. All the measurements were taken with the RF compensated Langmuir probe fixed at a distance of 30 mm above the powered electrode. Electron density of around 4.0×10^{16} m^{-3} and electron temperature of 3.0 eV was obtained from the probe measurement at 200 mTorr with 50 W RF power.

3.2. XPS, SIMS, AFM and hardness measurements

XPS spectra obtained by a broad energy scan show the presence of titanium (Ti 2p), nitrogen (N 1s) and oxygen (O 1s) on the surface of the treated samples. A representative spectrum is displayed in Fig. 2a. The C 1s photoelectron signal corresponds to the spurious surface carbon while the Si 2p and Si 2s signals are coming from the Si substrate. The XPS spectra corresponding to Ti 2p photoelectron signal for untreated as well as plasma treated Ti samples for different implantation times are

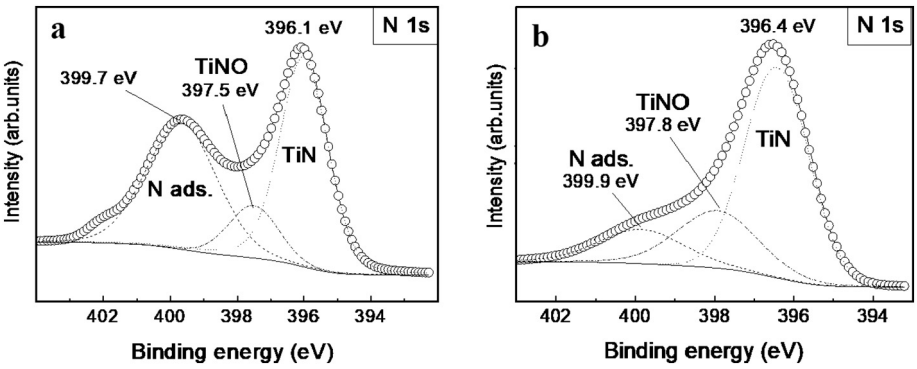

Fig. 5. High resolution XPS spectra of N 1s signal for the sample implanted for (a) 1 h duration and (b) 4 h duration.

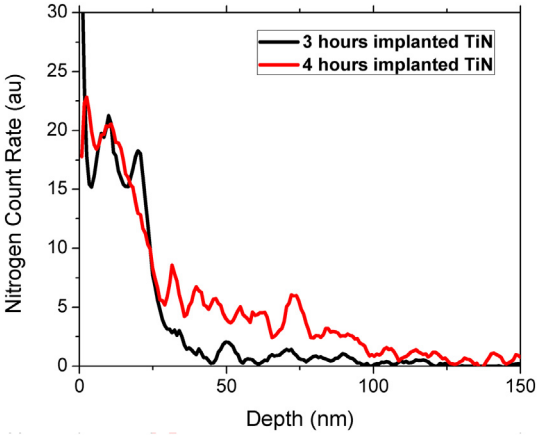

Fig. 6. SIMS spectrum for a sample with 3 h of implantation.

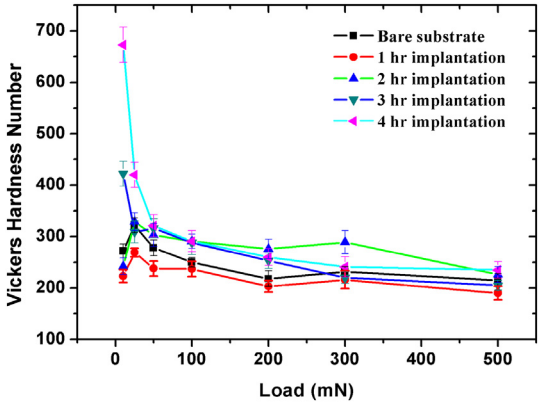

Fig. 8. Vickers micro-hardness for treated and untreated (bare) samples.

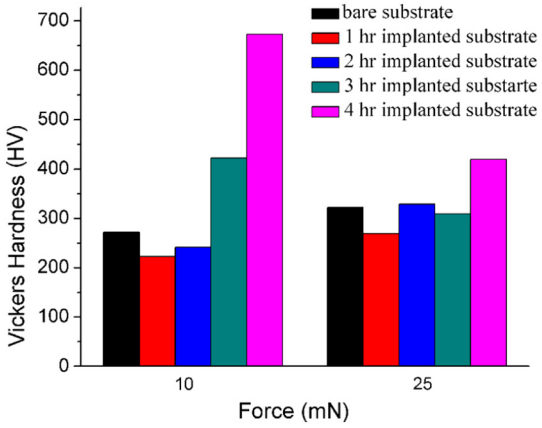

Fig. 9. Surface hardness of the untreated and PIII&D treated samples at different implementation times under two loads 10 mN and 25 mN.

shown in Fig. 2b. The signal corresponding to Ti $2p_{3/2}$ is observed between 453 and 461 eV, while $2p_{1/2}$ is observed between 462 and 468 eV. For the samples implanted for 2 h and above, a shoulder appears at about 455 eV, increasingly better defined for longer implantation time, which attributed to the TiN formation. While performing high resolution XPS analysis for Ti $2p_{3/2}$ peak, the titanium oxide (Ti(IV)−O bond) characteristic peak is observed at 458.4 eV [43–49] (see Fig. 3a and b). It was also noticed that an intermediate peak about 456.7 eV and a shoulder at 455.1 eV were also present [50,51]. The shoulder corresponds to TiN peak and its area as well as intensity increases with the treatment time. The peak observed at 456.7 eV corresponds to titanium oxynitride of the form TiO_xN_y [50,51]. The peak observed at the similar position for the untreated sample is reported as Ti_2O_3 [45,52]. Although pure Ti has a characteristic peak at about 454 eV [53,54], we have not observed it on the Ti 2p spectra probably due to the presence of native oxide on the surface. Analyzing high resolution Ti $2p_{3/2}$ spectra, it is possible to compare the relative percentages of TiN as compared with the ones associated to TiO_2 from the surface of the treated samples. The relative percentage was determined considering the area under the curve of the corresponding peaks. Fig. 4 shows the relative percentage of TiN and TiO_2 for different implantation time. This analysis indicates that with increasing implantation time, the relative percentage of TiN increases while that of TiO_2 decreases. This decrease in TiO_2 continues until 3 h of implantation after which the relative percentage of oxygen remained constant, which could indicate a (constant) reoxidation of the surface after venting the vacuum chamber. On the other hand, the relative percentage associated to titanium oxynitride increases with implantation time. Nitrogen has a characteristic peak for its pure state at about 398 eV [53]. In the high resolution XPS spectra shown in Fig. 5, it is observed that the N 1s peak of nitrogen can be decomposed into three separate peaks. The first and strongest peak located in the 396.1 eV (Fig. 5a) and 396.4 eV (Fig. 5b) is attributed to TiN presence [55]. The second peak at around 397.5 eV (Fig. 5a) and 397.8 eV (Fig. 5b) is attributed to titanium oxynitride [56]. The third peak at about 399.7 eV (Fig. 5a) and 399.9 eV (Fig. 5b) can be attributed to nitrogen adsorbed on the surface [57]. This analysis also reveals that with increasing implantation time, the relative percentage of area under the characteristic peak of TiN and titanium oxinitride increases. The results obtained from the N1s spectra agree well with the preceding analysis of the Ti $2p_{3/2}$ spectra. Fig. 6 shows penetration depth of the nitrogen ions implanted by PIII&D technique at two different implantation times obtained from SIMS measurements. It is observed that after 3 h of

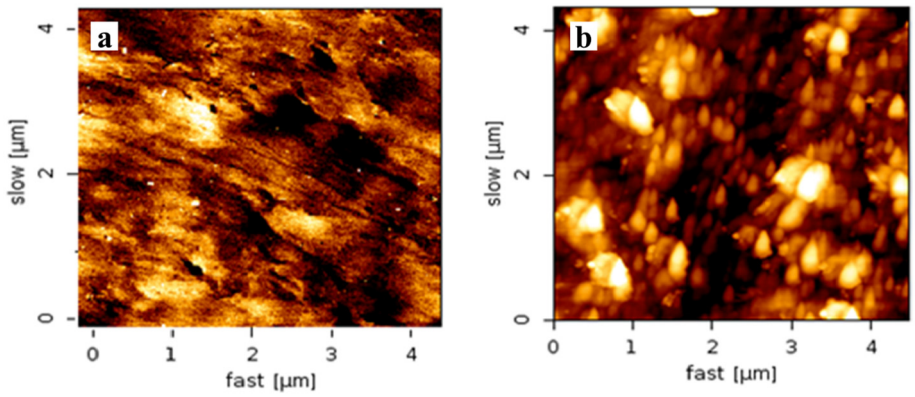

Fig. 7. AFM image of (a) polish titanium and (b) the ion-implanted titanium for 2 h.

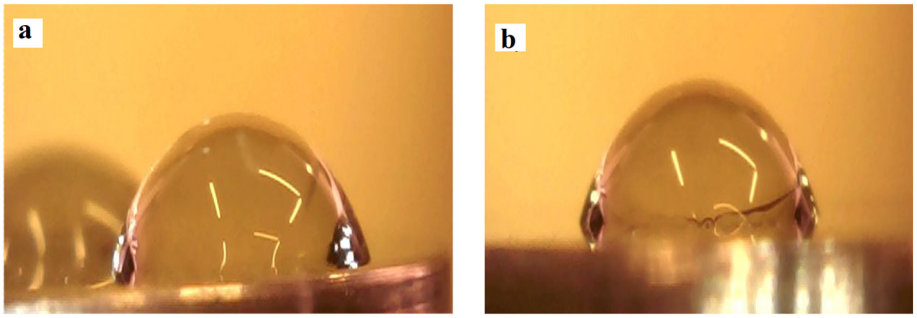

Fig. 10. (a) Contact angle of untreated Ti: 51 ± 8° and (b) PIII&D treated Ti: 52 ± 7°.

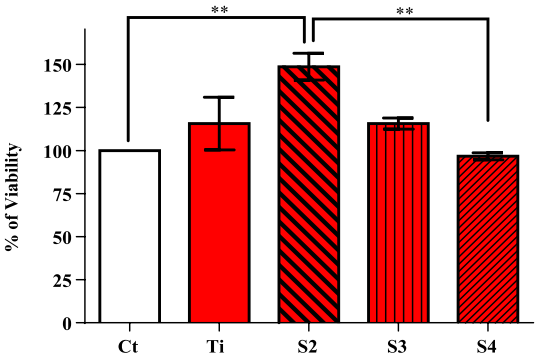

Fig. 11. Percentage of cell viability in the titanium plates without and with PIII &D treatment. The bars shows Mean ± SEM, $^{**}p < 0.01$ One way ANOVA.

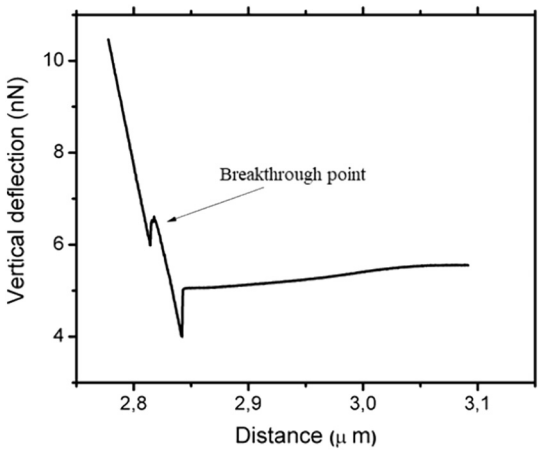

Fig. 13. AFM's tip force curve over the DPPC bilayer. The breakthrough point shows the rupture of the DPPC membrane due to the force applied by the AFM tip.

implantation, the penetration of nitrogen is up to about 40 nm while for the sample with 4 h of implantation, this depth increases to around 100 nm. It is important to mention here that an abundant presence of oxygen is being observed in the SIMS measurements. An explanation of this is the high temperature of the sample during the implantation treatment (~550 °C) and the presence of residual oxygen in the vacuum chamber, which may enhance the oxidation of the material and the diffusion of oxygen from the surface into the bulk. Fig. 7 shows AFM images of the samples before and after ion implantation for 2 h. After the ion implantation topographical changes on the surface of the Ti samples were observed. The surface roughness increases by a factor of 10 – from average roughness of 0.627 nm for a polish untreated Ti substrate to 6.55 nm – for the ion implanted Ti surface. Surface micro hardness was measured across the diameters (mean values averaged over a number of measurements) of the ion-implanted and un-implanted sample using a Vickers indenter under different load, from 10 mN to 500 mN. Fig. 8 shows the Vickers hardness of the un-implanted and ion-implanted samples for different implantation times under different loads. It has been observed that with increasing implantation time the surface hardness increases while using low load. This can be attributed to the rise of the nitrogen surface concentration with implantation time. For loads higher than 25 mN, the samples show similar hardness pattern for increasing loads. With increasing loads, the Vickers indenter breaks/penetrates through the thin TiN layer of the treated sample and therefore registers only the hardness of the sample material, or correspondingly the "Buckle rule" stating that the indentation depth must be < 10% of the layer thickness is violated. A comparative micro-hardness bar diagram at two different loads (10 and 25 mN) for the sample with different implantation times is shown in Fig. 9. It can be seen that the hardness increase occurs only at very low

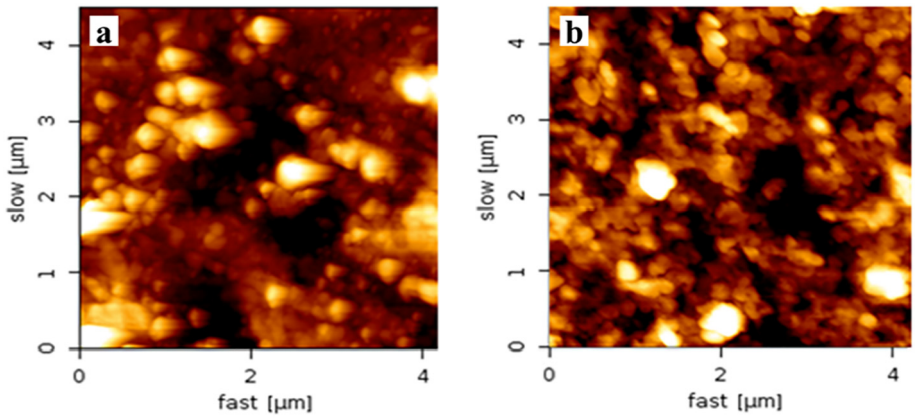

Fig. 12. Topographical image of CH evaporated over TiN (a) and DPPC evaporated over CH on TiN (b).

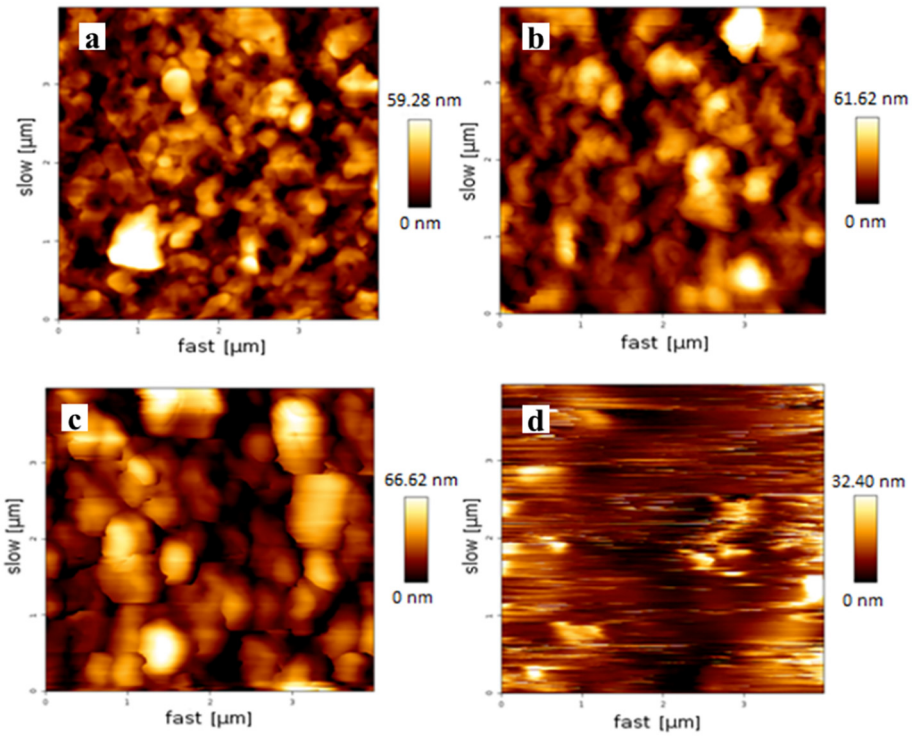

Fig. 14. AFM image for the DPPC at 24 °C (a), 38 °C (b), 47 °C (c) and 56 °C (d) at the same scanning area.

loads, which, along with the SIMS results, implies that the achieved implantation (and as such the formation of TiN) is very shallow. At 10 mN force on the sample implanted for 4 h the hardness increases to around 675 HV, equivalent to almost 2.5 times the hardness of the untreated sample, whereas at 25 mN it is almost 1.3 times the value of the untreated sample. It is important to consider that the bare polished samples did not receive a high temperature heat treatment (annealing), in contrast to the ion-implanted samples which have been heated in vacuum to 550 °C for 1, 2, 3 and 4 h, respectively during implantation process. It is known that the annealing process in metals reduces the hardness of the samples. It has been shown that the hardness of Ti material starts to decrease for samples annealed at 450 °C [58]. At higher annealing temperatures, the decrease in hardness or weakening of Ti is even more dramatic. Therefore, we conclude that our treated (annealed) bulk samples or substrates reduce their overall hardness due to the annealing procedure, in competition with the local increase of hardness in the thin TiN layer formed due to the ion implantation process. Our results show that for longer annealing times (3 and 4 h) the hardness in the thin nitrogen enriched surface region outperforms the overall weakening introduced to the bulk sample due to the annealing at 500 °C.

3.3. Bio-compatibility of PIII&D treated Ti

Modifying the titanium surface using plasma treatment is of great importance, but it should not degrade its initial bio-compatibility. The hydrophilicity of the treated and untreated surfaces was studied measuring the contact angle using a drop of ultrapure water. In Fig. 10 we observe that the treatment does not induce significant changes in the hydrophilicity of the sample, since its contact angle does not vary considerably. Once confirmed that the plasma treatment does not change the hydrophilicity of the sample, we proceeded to study the biocompatibility using a colorimetric analysis. This involves placing a certain amount of living cells on the substrate to be incubated at 37 °C for 24 h for observing how many of these cells are still alive on the substrate. This gives a measurement of the cell viability of implanted substrate compared to a not implanted substrate. It is possible to see the test results of cell viability in Fig. 11, where Ct is the number of initially deposited cells which are used as a reference and Ti is not implanted titanium sample. S2, S3 and S4 correspond to 2, 3 and 4 h plasma treated samples, respectively. Since we did not observe a decrease in the number of living cells, we conclude that the PIII&D treatment (TiN) does not change the cells viability and therefore, does not degrade the biocompatibility of the substrate. Interestingly a significant higher viability was observed for the cell associated to the sample plasma treated for 2 h, suggesting a better biocompatibility.

The artificial membrane was made in high vacuum ($\sim 10^{-6}$ Torr) using PVD monitored *in situ* with VHRE. The CH was evaporated and deposited as a thin layer on the TiN substrate forming large agglomerations of CH on top of this homogeneous layer [59] (Fig. 12a). Subsequently, a thin membrane of DPPC was evaporated on the CH coated TiN substrate (Fig. 12b). The average roughness for the CH/TiN was 25.69 nm, while for the DPPC/CH/TiN it was 10.86 nm. Because of this increasing smoothening of the films, we conclude that part of DPPC is deposited in-between the CH agglomerations (see Fig. 12). To confirm the proper formation of the artificial membrane, AFM force curves were performed to break through the membrane due to the pressure of the tip. The AFM tip can only break through the DPPC membrane, because CH and titanium are harder than the silicon tip of the AFM. If the force curve shows the breakup or breakthrough, it indicates that the SLB membrane was formed. Fig. 13 shows that the breakup of the membrane occurred and it is possible to measure the depth of the tip jump, obtaining a value close to 3.34 nm, corresponding to the thickness of the SLB membrane (3.34 nm is the difference in distance, measured between the maximum and relative minimum at a distance of 2.8 µm from the surface). A complementary way to detect the formation of an artificial membrane is by observing the topographical changes in AFM images taken at different temperatures. Fig. 14 shows the membrane in different phases. Specifically, the Fig. 14a and b show the DPPC in the gel phase at 24 °C and the ripple phase at 38 °C, resp. Due to the mobility acquired by the membrane molecules during the increase of the temperature, it is possible to notice a small increment in the maximum

height of the sample. Fig. 14c and d show the DPPC in the fluid phase at 47 °C and the fluid disordered phase at 56 °C, resp. At these temperatures the DPPC begins to lose the bilayer structure [4,59], due to the high mobility of the molecules that compose the DPPC bilayer. The fluid disordered phase is clearly observed. In this phase it is not possible to detect any surface structure, in contrast to the DPPC SLB over CH on TiN at lower temperatures (see Fig. 12).

4. Conclusion

This paper confirms the implantation of nitrogen onto polished titanium substrate using PIII&D technique with capacitively coupled radio frequency plasma. The maximum depth of nitrogen ion penetration was 180 nm for 4 h of implantation time at 500 °C. For this reason, the increment of hardness only occurs for low loads (10 mN). With XPS the formation of TiN was confirmed on the sample surface. A calorimetric assay confirms the biocompatibility of the implanted samples in the same way as for the un-treated titanium with the native oxide layer. Using AFM not only morphological changes representative for an increment in the roughness of the sample were observed, but it was also possible to confirm the artificial membrane formation using temperature ramps and force curves. This research confirms that the nitrogen PIII&D treated Ti can be used to support stable phospholipid artificial membranes (SLBs) with enhanced biocompatibility, deposited in high vacuum from their gas phase.

Acknowledgement

Authors acknowledge FONDECYT grant 1170261, 3160179, 1180939 and 3160803. Additional funding from CONICYT PIA program ACT 1107 and ACT 1108 is acknowledged. MC acknowledges CONICYT Master Scholarships.

References

[1] S.L. Duncan, I.S. Dalal, R.G. Larson, Molecular dynamics simulation of phase transitions in model lung surfactant monolayers, Biochim. Biophys. Acta 1808 (10) (2011) 2450–2465.
[2] C.B. Fox, R.H. Uibel, J.M. Harris, Detecting phase transitions in phosphatidylcholine vesicles by Raman microscopy and self-modeling curve resolution, J. Phys. Chem. B 111 (2007) 11428–11436.
[3] C.H. González, U.G. Volkmann, M.J. Retamal, M. Cisternas, M.A. Sarabia, K.A. López, Thermal behavior of 1,2-dipalmitoyl-sn-3-phosphoglycerocholine bi- and multi-layers, deposited with physical vapor deposition under ellipsometric growth control, J. Chem. Phys. 136 (13) (2012) 134709.
[4] M.J. Retamal, M.A. Cisternas, S.E. Gutierrez-Maldonado, T. Perez-Acle, B. Seifert, M. Busch, P. Huber, U.G. Volkmann, Towards bio-silicon interfaces: formation of an ultra-thin self-hydrated artificial membrane composed of dipalmitoylphosphatidylcholine (DPPC) and chitosan deposited in high vacuum from the gas-phase, J. Chem. Phys. 141 (10) (2014) 104201.
[5] M. Geetha, A.K. Singh, R. Asokamani, A.K. Gogia, Ti based biomaterials, the ultimate choice for orthopaedic implants — a review, Prog. Mater. Sci. 54 (3) (2009) 397–425.
[6] X. Liu, P.K. Chu, C. Ding, Surface modification of titanium, titanium alloys, and related materials for biomedical applications, Mater. Sci. Eng. R Rep. 47 (2004) 49–121, 2004.
[7] M. Cisternas, F. Mellero, M. Favre, H. Bhuyan, E. Wyndham, TiN coatings on titanium substrates using plasma assisted ion implantation, J. Phys. Conf. Ser. 591 (2015) 012043.
[8] W. Ding, Q. Lian, R.J. Samuels, M.B. Polk, Synthesis and characterization of a novel derivative of chitosan, Polymer (Guildf) 44 (2002) 547–556.
[9] Y. Zhao, S.M. Wong, H.M. Wong, et al., Effects of carbon and nitrogen plasma immersion ion implantation on in vitro and in vivo biocompatibility of titanium alloy, ACS Appl. Mater. Interfaces 5 (2013) 1510–1516.
[10] T. Sun, L.P. Wang, M. Wang, H.W. Tong, W.W. Lu, PIIID-formed (Ti, O)/Ti, (Ti, N)/Ti and (Ti, O, N)/Ti coatings on NiTi shape memory alloy for medical applications, Mater. Sci. Eng. C 32 (2012) 1469–1479.
[11] T. Sun, L.P. Wang, M. Wang, (Ti, O)/Ti and (Ti, O, N)/Ti composite coatings fabricated via PIIID for the medical application of NiTi shape memory alloy, J Biomed Mater Res B Appl Biomater 96 (2011) 249–260.
[12] L. Gence, M. Escalona, C Castillo, *et al.*, "Wrinkled titanium nitride nanocomposite for robust bendable electrodes", Nanotechnology, vol. 30, pp. 495705.
[13] W.J. Meng, T.J. Curtis, Inductively coupled plasma assisted physical vapor deposition of titanium nitride coatings, J. Elect. Mater. 26 (1997) 1297–1302.
[14] G.M. Ingo, S. Kaciulis, A. Mezzi, T. Valente, F. Casadei, G. Gusmano, Characterization of composite titanium nitride coatings prepared by reactive plasma spraying, Electrochim. Acta 50 (23) (Aug. 2005) 4531–4537.
[15] P. Saikia, A. Joseph, R. Rane, B. Saikia, S. Mukherjee, Role of substrate and deposition conditions on the texture evolution of titanium nitride thin film on bare and plasma-nitrided high-speed steel, J. Theor. Appl. Phys. 7 (1) (2013) 66.
[16] H. Bhuyan, S. Mändl, B. Bora, M. Favre, E. Wyndham, J.R. Maze, M. Walczak, D. Manova, Surface modification by nitrogen plasma immersion ion implantation into new steel 460Li-21Cr in a capacitively coupled radio frequency discharge, Appl. Surf. Sci. 316 (2014) 72–77.
[17] Z. Xie, L. Wang, X. Wang, L. Huang, Y. Lu, J. Yan, Mechanical performance and corrosion behavior of TiAlSiN/WS_2multilayer deposited by multi-plasma immersion ion implantation and deposition and magnetron sputtering, Trans. Nonferrous Metals Soc. China 21 (2011) s476–s482.
[18] Y. Cheng, Y.F. Zheng, Surface characterization and mechanical property of TiN/Ti-coated NiTi alloy by PIIID, Surf. Coat. Technol. 201 (2007) 6869–6873.
[19] M. Zhang, X.H. Li, Y.D. Gong, N.M. Zhao, X.F. Zhang, Properties and biocompatibility of chitosan films modified by blending with PEG, Biomaterials 23 (2002) 2641–2648.
[20] C. Peniche, W. Argüelles-Monal, H. Peniche, N. Acosta, Chitosan: an attractive biocompatible polymer for microencapsulation, Macromol. Biosci. 3 (2003) 511–520.
[21] D.S. Couto, Z. Hong, J.F. Mano, Development of bioactive and biodegradable chitosan-based injectable systems containing bioactive glass nanoparticles, Acta Biomater. 5 (2009) 115–123.
[22] M.E. López-Caballero, M.C. Gómez-Guillén, M. Pérez-Mateos, P. Montero, A chitosan-gelatin blend as a coating for fish patties, Food Hydrocoll. 19 (2005) 303–311.
[23] E.I. Rabea, M.E.T. Badawy, C.V. Stevens, G. Smagghe, W. Steurbaut, Chitosan as antimicrobial agent: applications and mode of action, Biomacromolecules 4 (6) (2003) 1457–1465.
[24] A. El Hadrami, L.R. Adam, I. El Hadrami, F. Daayf, Chitosan in plant protection, Mar. Drugs 8 (2010) 968–987.
[25] T. Masuko, A. Minami, N. Iwasaki, T. Majima, S.I. Nishimura, Y.C. Lee, Thiolation of chitosan. Attachment of proteins via thioether formation, Biomacromolecules 6 (2005) 880–884.
[26] X.G. Chen, L. Zheng, Z. Wang, C.Y. Lee, H.J. Park, Molecular affinity and permeability of different molecular weight chitosan membranes, J. Agric. Food Chem. 50 (2002) 5915–5918.
[27] M. Burkatovskaya, A.P. Castano, T.N. Demidova-Rice, G.P. Tegos, M.R. Hamblin, Effect of chitosan acetate bandage on wound healing in infected and noninfected wounds in mice, Wound Repair Regen. 16 (2008) 425–431.
[28] Y. Pan, Y.Z. Zhang, Y. Li, Layer-by-layer self-assembled multilayer films of single-walled carbon nanotubes and tin disulfide nanoparticles with chitosan for the fabrication of biosensors, J. Appl. Polym. Sci. 128 (2013) 647–652.
[29] K. Zhou, Y. Zhu, X. Yang, J. Luo, C. Li, S. Luan, A novel hydrogen peroxide biosensor based on Au-graphene-HRP-chitosan biocomposites, Electrochim. Acta 55 (2010) 3055–3060.
[30] D. Thacharodi, K.P. Rao, Development and in vitro evaluation of chitosan-based transdermal drug delivery systems for the controlled delivery of propranolol hydrochloride, Biomaterials 16 (2) (1995) 145–148.
[31] N.M. El-Sawy, H.a. Abd El-Rehim, A.M. Elbarbary, E.S. a Hegazy, Radiation-induced degradation of chitosan for possible use as a growth promoter in agricultural purposes, Carbohydr. Polym. 79 (3) (2010) 555–562.
[32] S. Roller, N. Covill, The antifungal properties of chitosan in laboratory media and apple juice, Int. J. Food Microbiol. 47 (1999) 67–77.
[33] O. B. G. Assis, R. Bernardes-Filho, D. C. Vieira, and S. P. C. Filho, "AFM characterization of chitosan self-assembled films," Int. J. Polym. Mater., vol. 51, no. April 2015, pp. 633–638, 2002.
[34] R.Y.M. Huang, G.Y. Moon, R. Pal, Chitosan/anionic surfactant complex membranes for the pervaporation separation of methanol/MTBE and characterization of the polymer/surfactant system, J. Membr. Sci. 184 (2001) 1–15.
[35] A. Heras, N.M. Rodríguez, V.M. Ramos, E. Agulló, N-methylene phosphonic chitosan: a novel soluble derivative, Carbohydr. Polym. 44 (2001) 1–8.
[36] V. M. Ramos, N. M. Rodríguez, M. F. Díaz, M. S. Rodríguez, A. Heras, and E. Agulló, "N-methylene phosphonic chitosan. Effect of preparation methods on its properties, " Carbohydr. Polym., vol. 52, pp. 39–46, 2003.
[37] M.R. Morrow, J. Stewart, S. Taneva, A. Dico, K.M.W. Keough, Perturbation of DPPC bilayers by high concentrations of pulmonary surfactant protein SP-B, Eur. Biophys. J. 33 (2004) 285–290.
[38] B. Pawlikowska-Pawlęga, L.E. Misiak, B. Zarzyka, R. Paduch, A. Gawron, W.I. Gruszecki, Localization and interaction of genistein with model membranes formed with dipalmitoylphosphatidylcholine (DPPC), Biochim. Biophys. Acta Biomembr. 1818 (2012) 1785–1793.
[39] F.M. El-Hossary, A.M. Abd El-Rahman, M. Raaif, D.A. Ghareeb, Properties of TiAlN coating deposited by MPIIID on TiN substrates, Appl. Phys. A Mater. Sci. Process. 122 (2016) 242.
[40] T. Mosmann, Rapid colorimetric assay for cellular growth and survival: application to proliferation and cytotoxicity assays, J. Immunol. Methods 65 (1–2) (1983) 55–63.
[41] S. Mändl, J. Lutz, C. Díaz, J.W. Gerlach, J.A. García, Influence of reduced current density on diffusion and phase formation during PIII nitriding of austenitic stainless steel and CoCr alloys, Surf. Coat. Technol. 256 (2014) 78–84.
[42] L. Oksuz, N. Hershkowitz, Plasma, presheath, collisional sheath and collisionless sheath potential profiles in weakly ionized, weakly collisional plasma, Plasma Sources Sci. Technol. 14 (2005) 201–208.
[43] I. Bert, M. Mohai, J.L. Sullivan, S.O. Saied, Surface characterisation of plasma-nitrided an XPS study titanium, Appl. Surf. Sci. 84 (1995) 357–371.

[44] F.-H. Lu, H.-Y. Chen, Characterization of titanium nitride films deposited by cathodic arc plasma technique on copper substrates, Surf. Coat. Technol. 130 (2000) 290–296.
[45] C.L. Liang, G.A. Cheng, R.T. Zheng, H.P. Liu, J.C. Li, H.F. Zhang, G.J. Ma, Y.L. Jiang, Composition and texture of TiN thin films fabricated by ECR enhanced sputtering deposition, Surf. Coat. Technol. 201 (2007) 5537–5540.
[46] Y. Cheng, Y.F. Zheng, Surface characterization and mechanical property of TiN/Ti-coated NiTi alloy by PIIID, Surf. Coat. Technol. 201 (2007) 6869–6873.
[47] M.V. Kuznetsov, J.F. Zhuravlev, V.a. Zhilyaev, V.a. Gubanov, XPS study of the nitrides, oxides and oxynitrides of titanium, J. Electron. Spectrosc. Relat. Phenom. 58 (1992) 1–9.
[48] R. Ohnishi, M. Katayama, D. Cha, K. Takanabe, J. Kubota, K. Domen, Titanium nitride nanoparticle electrocatalysts for oxygen reduction reaction in alkaline solution, J. Electrochem. Soc. 160 (6) (2013) F501–F506.
[49] I. Milosev, H.-H. Strehblow, B. Navinses, M. Metikos-Huković, Electrochemical and thermal oxidation of TiN coatings studied by {XPS}, Surf. Interface Anal. 23 (1995) 529–539 no. March.
[50] K.S. Robinson, P.M.A. Sherwood, X-ray Photoelectron Spectroscopic Studies of the Surface of Sputter Ion Plated Films, no. 6 (1984), pp. 3–8.
[51] S. Hofmann, Characterization of nitride coatings by Auger electron spectroscopy and x-ray photoelectron spectroscopy, J. Vacc. Sci. Technol. A Vacuum, Surfaces, Film. 4 (May 2013) (1986) 2789.
[52] I. Strydom, S. Hofmann, TII Contribution of Characteristics Energy Losses in the Core-level X-ray Photo Electron Spectroscopy Peaks of TiN and (Ti, Al)N Studied by Electron Energy Loss Spectroscopy and X-ray Photoelectron Spectroscopy, 56 (1991), pp. 85–103.
[53] J.F. Moulder, W.F. Stickle, P.E. Sobol, K.D. Bomben, X-ray Photoelectron Spectroscopy, (1992).
[54] E. Galvanetto, F.P. Galliano, F. Borgioli, U. Bardi, A. Lavacchi, XRD and XPS study on reactive plasma sprayed titanium-titanium nitride coatings, Thin Solid Films 384 (2001) 223–229.
[55] F. Esaka, Comparison of surface oxidation of titanium nitride and chromium nitride films studied by X-ray absorption and photoelectron spectroscopy, J. Vac. Sci. Technol. A Vac. Surf. Film 15 (1997) 2521, 1997.
[56] I. Bertoti, M. Mohai, J.L. Sullivan, S. Said, Surface chemical changes in PVD TiN layers induced by ion bombardment, Surf. Interface Anal. 21 (1994) 467–473.
[57] K.S. Robinson, P.M.A. Sherwood, X-ray photoelectron spectroscopic studies of the surface of sputter ion plated films, 6 (1984) 3–8.
[58] Yongzhou Wang, Master theses at School of Materials of the Faculty of Engineering and Physical Sciences, University of Manchester, https://www.research.manchester.ac.uk/portal/files/54557993/FULL_TEXT.PDF, (2014).
[59] M.J. Retamal, T.P. Corrales, M.A. Cisternas, N.H. Moraga, D.I. Diaz, R.E. Catalan, B. Seifert, P. Huber, U.G. Volkmann, Surface morphology of vapor-deposited chitosan: evidence of solid-state dewetting during the formation of biopolymer films, Biomacromolecules 17 (2016) 1142–1149.